Optics Letters

# Energy deposition of single femtosecond filaments in the atmosphere

E. W. Rosenthal, N. Jhajj, I. Larkin, S. Zahedpour, J. K. Wahlstrand, and H. M. Milchberg*

*Institute for Research in Electronics and Applied Physics, University of Maryland, College Park, Maryland 20742, USA*
**Corresponding author: milch@umd.edu*

*Received 24 June 2016; revised 22 July 2016; accepted 1 August 2016; posted 1 August 2016 (Doc. ID 269180); published 15 August 2016*

**We present spatially resolved measurements of energy deposition into atmospheric air by femtosecond laser filaments. Single filaments formed with varying laser pulse energy and pulsewidth were examined using longitudinal interferometry, sonographic probing, and direct energy loss measurements. We measure peak and average energy absorption of ~4 μJ/cm and ~1 μJ/cm for input pulse powers up to ~6 times the critical power for self-focusing.** 

***OCIS codes:*** (010.1290) Atmospheric optics; (010.1300) Atmospheric propagation; (260.2160) Energy transfer; (320.7110) Ultrafast nonlinear optics.

http://dx.doi.org/10.1364/OL.41.003908

Femtosecond filamentation is a nonlinear propagation effect in transparent media caused by the dynamic interplay between self-focusing and plasma-induced defocusing. In recent years it has found a variety of uses, including triggering of electric discharges [1], coherent supercontinuum generation [2], filament-induced breakdown spectroscopy [3], and generation of THz radiation [4]. More recently, femtosecond filaments have been used to generate air waveguides, utilizing the long timescale gas density depression that remains in the wake of a filamenting pulse [5]. Such waveguides have been shown to be viable for the guiding of externally injected high-peak and high-average-power laser pulses [5], and also for the remote collection of optical signals for spectral analysis [6]. Crucial to these schemes is the nonlinear deposition of energy into the propagation medium, the magnitude and distribution of which determines the depth and axial extent of the index perturbation constituting the air waveguide. Because such waveguides are generated using multi-filamenting beams generated by the collapse of higher-order transverse modes [5,7], a basic goal is to determine the energy deposition per unit length of propagation for a single filament. Our results presented in this Letter are distinct from other recent measurements [8–11] of laser propagation and absorption under tight (non-filamentary) focusing of an ultrashort pulse in air, where because the focusing is lens-dominated rather than nonlinearity-dominated, the pulse intensity can exceed the typical clamping intensity in air of $\sim 5 \times 10^{13}$ W/cm$^2$ [12], with an attendant significant increase in gas ionization and laser absorption.

As a filamenting pulse propagates through the atmosphere, it deposits energy into the propagation medium through optical field ionization and by non-resonant rotational Raman excitation of the air molecules [13]. Other energy deposition channels are present, but are comparatively negligible: heating by above-threshold ionization, whereby a photo-ionized electron is born with nonzero kinetic energy [14], and inverse bremsstrahlung heating by laser-driven electron-ion collisions in the dilute filament plasma [15]. All of the direct excitations of the air by the filament are eventually converted to a localized distribution of thermal energy of neutral air [16]; the weakly ionized plasma channel produced by the filamenting pulse recombines in less than ~10 ns [17], and the rotational excitation collisionally decoheres on a ~100 ps timescale [18]. These times are much faster than the acoustic response timescale of the filament-heated gas, $\tau_a \sim a/c_s$, ~300 ns, where $a \sim$ 100 μm is the filament diameter and $c_s \sim 3 \times 10^4$ cm/s is the sound speed in ambient air. Femtosecond filament heating of air creates a narrow and elongated region of elevated thermal energy density that impulsively drives an outwardly propagating single-cycle acoustic wave [7,16], leaving behind a long-lived gas density depression, or "density hole," which dissipates on millisecond timescales by thermal diffusion [16].

It is first useful to assess the fraction of absorbed laser energy that goes into the acoustic wave. Once the single-cycle acoustic wave propagates away from the laser-heated volume, the gas is in pressure balance (that is, the pressure is uniform), leaving an elevated temperature and reduced density at the density hole, with the temperature and density transitioning to ambient atmospheric temperature and density outside the hole [7,16]. For an ideal diatomic gas for which only translational and rotational degrees of freedom are available, the thermal energy density is related to the pressure by $\epsilon = (5/2)P$. (The filament-induced gas temperature rise is insufficient to excite vibrations). Thus, after the acoustic wave propagates away, the energy density throughout the region is constant and equal to its pre-laser heating value. We therefore infer that the acoustic wave carries away nearly 100% of the energy invested in the gas by the laser pulse. Other possible energy dissipation channels are thermal radiation and thermal conduction. For the initial filament-induced temperature increase of $\Delta T \sim 100$ K [16], thermal

radiation is negligible, and on the ~1 μs timescale over which the acoustic wave propagates away, thermal conduction has had little time to affect the energy balance [16].

The above analysis shows that two independent methods can be used as proportional measures of laser energy absorption: microphone measurements of the acoustic wave, and interferometric measurement of the density hole remaining after the acoustic wave propagates away. If the initial absorbed energy density from the filament is $\Delta\epsilon_i = (5/2)\Delta P_i$, where $\Delta P_i = N_0 k_B \Delta T_i$ is the initial pressure increase upon laser heating, $N_0$ is the ambient air density, $\Delta T_i$ is the initial temperature increase, and $k_B$ is Boltzmann's constant, a microphone placed a fixed short distance R from the filament will register a peak signal amplitude $\delta S_{\mathrm{mic}} \propto \Delta P_i / R^{1/2} \propto \Delta\epsilon_i$, a proportional measure of laser energy absorption. Meanwhile, the residual density hole left behind by the acoustic wave has a maximum initial depth $\Delta N_i = -\Delta T_i (N_0/T_0)$, which later evolves as $\Delta N(t) = -\Delta T(t)(N_0/T_0)$ as the temperature relaxes to the ambient value $T_0$ by thermal diffusion [16]. Therefore, an interferometric measurement of the depth of the density hole at a fixed delay, after the acoustic wave has left, is also a proportional measure of the initial laser energy absorption.

The experimental setup is shown in Fig. 1, incorporating interferometric and microphone measurements of filament absorption [Fig. 1(a)], as well as a third independent technique, a direct measurement of absorption using a broadband photodiode and integrating sphere [Fig. 1(b)]. Up to ~2 m long filaments were generated by weakly focusing $\lambda = 800$ nm Ti:Sapphire laser pulses at $f/600$ with an $f = 3$ m $MgF_2$ lens. Incident pulse energy was varied by passing the beam through a motorized waveplate followed by two reflections from thin film polarizers, allowing excellent polarization contrast and fine

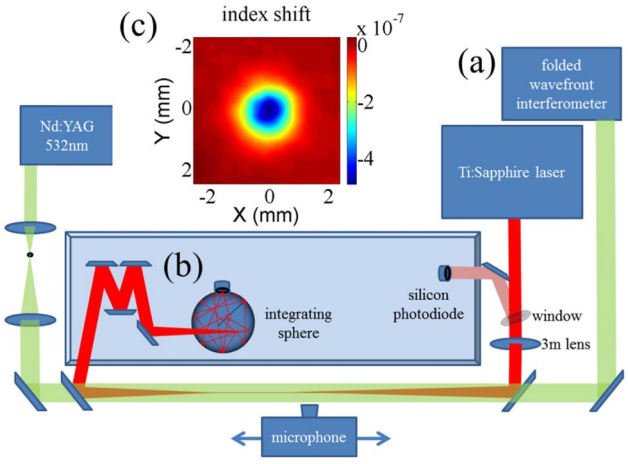


**Fig. 1.** (a) Pulses from a 10 Hz, 800 nm, Ti:sapphire amplifier are focused at $f/600$ by an $f = 3$ m $MgF_2$ lens to form a single filament of length <2 m. (a) A 7 ns, 532 nm interferometer probe pulse (variably delayed between 2–5 ms) is propagated longitudinally along the filament-induced density hole and into a folded wavefront interferometer for retrieval of $\overline{\Delta n}(\mathbf{r}_\perp)$, the axially averaged refractive index shift profile. The inset, (c), shows a typical $\overline{\Delta n}(\mathbf{r}_\perp)$ profile obtained from a 100-shot averaged phase shift profile. (b) Part of the incident pulse energy is measured by a reference Si photodiode. After filament termination, the far-field beam mode is near-normally reflected by a sequence of wedges and collected by an integrating sphere, enabling a direct, broadband, and sensitive measurement of absorbed energy.

pulse energy variation between 0 and 4 mJ. Pulsewidth was varied by changing the compressor grating separation. Examination of the beam with a card along the filament ensured that for all pulse energies chosen, propagation was in the single filament regime.

For the direct absorption measurements [Fig. 1(b)], reflection from a thin glass window prior to the start of filamentation gives a reference photodiode signal proportional to the incident pulse energy. In the far-field, after self-termination of the filament, the beam is attenuated by near-normal incidence reflections (<3° from normal) from a series of glass wedges and sent into an integrating sphere with an identical photodiode. The UV-enhanced silicon photodiodes have a relatively flat spectral response in the visible/NIR spectral region, as do the near-normal incidence wedge reflections and the integrating sphere internal coating. This setup accommodates the extreme spectral broadening induced by filamentation.

The reference and integrating sphere photodiode signals were absolutely calibrated against a commercial laser energy meter and relatively calibrated against each another using a long-pulse (~10 ns), low-energy, linearly propagating (non-filamenting) beam, derived from the Ti:Sapphire laser with the oscillator seed pulse blocked. The photodiode signals were found to be linearly proportional to each other and to the incident pulse energy to within 1% throughout the entire range of energies used in our experiments.

Direct absorption measurements are plotted in Fig. 2 as a function of incident pulse energy for a range of pulsewidths. The highest absorption of ~4% (~200 μJ) is observed for the shortest and highest energy pulse (50 fs, 4 mJ). The data points are replotted on log–log scales in the inset, where dashed lines following energy (or intensity $I$) squared dependences are overlaid. It is seen in all plots that absorption for the low- to mid-range of pulse energies (indicated by left- and right-hand vertical dashed lines) is well-described by an $I^2$ dependence, with faster variation at higher energies. Note that the left-hand

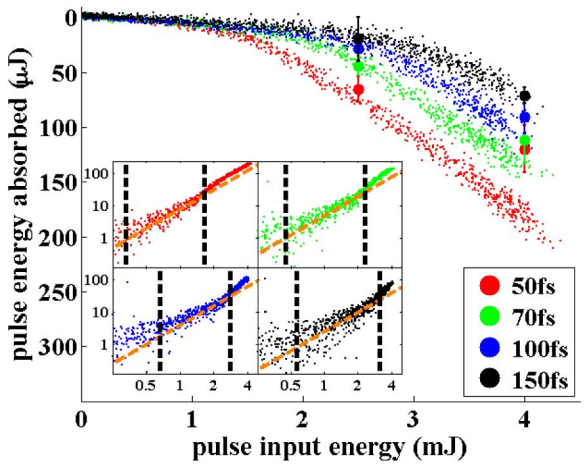


**Fig. 2.** Laser pulse energy absorbed in single filamentation versus input pulse energy, as measured using a pair of calibrated photodiodes in the configuration of Fig. 1(b). Overlaid points represent measurements of total energy absorption, $E_{\mathrm{abs}}$, determined by longitudinal interferometry. Error bars on those points are the differences between largest and smallest measured absorptions. Inset: data points of (a) replotted on a log–log scale, overlaid with dashed lines depicting absorption $\propto I^2$.

dashed line extends to lower energies for shorter pulsewidths, consistent with the wider range of intensities available in those cases. The $I^2$ absorption dependence is consistent with gas absorption by non-resonant two-photon rotational Raman excitation in nitrogen and oxygen, as discussed in [13,18,19]. At pulse energies beyond the right-hand dashed line, the absorption is seen to grow faster than $I^2$, in accord with the onset of plasma generation and additional heating, and then saturate (in the highest peak intensity 50 fs and 70 fs cases) owing to the limitation of laser intensity by plasma defocusing, or intensity clamping [12].

The gas hydrodynamic response, from which we infer the laser energy absorption, was first measured interferometrically and then sonographically. A variably delayed 7 ns, 532 nm probe pulse counter-propagating with respect to the filament [see Fig. 1(a)] provided time-resolved interferometric measurements of the propagation path-averaged gas density depression in the long time delay thermal regime (a few milliseconds). In this regime, the mild transverse gas density gradients minimize refraction and distortion of the probe. Beam propagation simulations [20] verify that the maximum phase error introduced by probe refraction over ~2 m filaments is <5% for our experimental parameters. To enable quasi-real-time background subtraction for interferometric phase extraction, the prefilamenting beam is passed through an optical chopper with a 50% duty cycle, alternating shots with and without the filament.

Interferograms were analyzed using standard techniques [21] to extract the 2D spatial phase pattern $\Delta\Phi(\mathbf{r}_\perp) = k\int_0^L dz\Delta n(\mathbf{r}_\perp, z)$ imposed on the probe beam by its passage through the filament-induced gas density hole. Here, $\Delta n$ is the air index change resulting from the gas density hole, $z$ is the filament propagation coordinate, $\mathbf{r}_\perp$ is the transverse coordinate, $L$ is the filament length, and $k$ is the probe beam vacuum wavenumber.

The initial energy density increase from filament heating can also be written $\Delta\epsilon_i = \rho_0 c_v \Delta T_i$, where $c_v$ is the specific heat capacity of air at constant volume, $\rho_0$ is the initial air mass density, and where $\int d^2\mathbf{r}_\perp dz\Delta\epsilon_i(\mathbf{r}_\perp, z) = E_{\text{abs}}$, the total absorbed energy. Immediately after the acoustic wave has propagated away and pressure equilibrium is established, the initial mass density distribution of the density hole follows $\Delta\rho_i = -\Delta T_i(\rho_0/T_0) = -\Delta\epsilon_i/c_v T_0$. As the temperature profile relaxes by thermal diffusion, we can *define* an energy density $\Delta\epsilon(\mathbf{r}_\perp, z, t) = -c_v\Delta\rho(\mathbf{r}_\perp, z, t)T_0$ which has the property $\int d^2\mathbf{r}_\perp dz\Delta\epsilon(\mathbf{r}_\perp,z,t) = -c_v T_0\int d^2\mathbf{r}_\perp dz\Delta\rho(\mathbf{r}_\perp,z,t) = E_{\text{abs}}$ independent of delay. In effect, the magnitude of the energy deposition is encoded in the density profile that remains in the filament's wake after the acoustic wave propagates away. Using $\Delta\rho = \rho_0\Delta n/(n-1)$, where $n$ is the air refractive index [22], the total energy loss along the filament is then $E_{\text{abs}} = -c_v T_0\rho_0 k^{-1}(n-1)^{-1}\int d^2\mathbf{r}_\perp\Delta\Phi(\mathbf{r}_\perp)$, where $T_0 = 297$ K and $\Delta\Phi(\mathbf{r}_\perp)$ is determined by interferometry, as discussed.

Interferometry-extracted values of total energy absorption are overlaid on the curves of Fig. 2 using two input energies and four probe delays at each energy. The error bars are the difference between the largest and smallest measured absorptions. These values for absorption are in reasonable agreement with those obtained directly using the photodiode arrangement of Fig. 1(b), except that they are consistently smaller, especially for the highest intensity pulses where the direct absorption and interferometry results differ by ~30%. We are currently investigating this discrepancy, which points to a loss mechanism at the highest intensities not contributing to thermal heating.

While the interferometry experiment provides overall energy absorption, detailed longitudinal dependence of energy absorption was performed using sonographic probing, a technique used in several filament-related experiments [7,9,15,19,23]. Here, a compact electret-type microphone was scanned alongside the filament at a transverse distance of $R = 1.5$ mm along its entire longitudinal extent. The microphone signal, $\delta S_{\text{mic}} \propto \Delta P_i/R^{1/2} \propto \Delta\epsilon_i$, was collected at 2 cm steps along the filament.

Figure 3 shows longitudinal distributions of energy deposition per unit length $dE_{\text{abs}}/dz$ for a range of sonographically probed filaments, where the vertical scale is set by $E_{\text{abs}}$ as determined by the longitudinal interferometry experiment, so that Fig. 3 is a purely hydrodynamically determined result. The values for $E_{\text{abs}}$ are in reasonable agreement with the direct absorption measurements of Fig. 2. Alternatively, the vertical scales of Fig. 3 could have been set by the direct absorption measurements. We note that our results for $dE_{\text{abs}}/dz$ are more in line with the long pulse simulation results of Ref. [15] at $f/500$ than the short pulse results in that Letter. An important question is the dependence of absorption on f-number. We have found through propagation simulations [15] that the peak absorption rate in μJ/cm can drop by a factor of two over the range $f/600 \rightarrow f/\infty$, with average absorption roughly constant.

For application of filament absorption to air waveguide generation, it is useful to consider what limits the length of

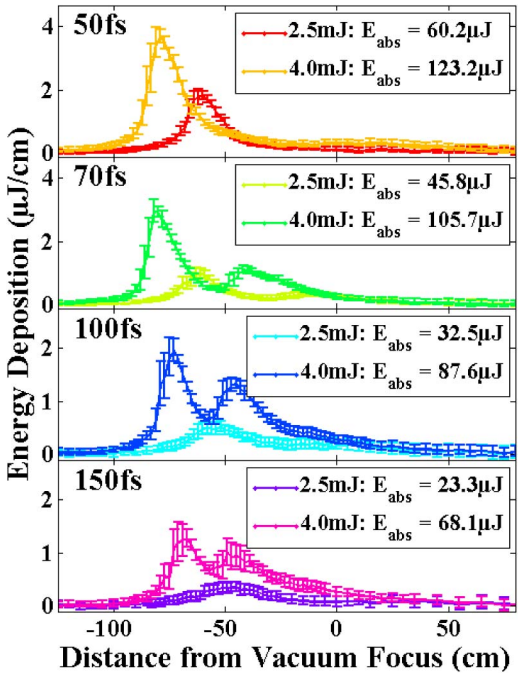


**Fig. 3.** Sonographic maps of the linear energy deposition versus position along the filament. The geometric focus of the $f/600$ optics is at $z = 0$. At each position in the axial scan, 100 shots were taken. The error bars are the standard deviation of the peak microphone signal at each position. The values of $E_{\text{abs}}$ in the legend are integrals of each curve.

a single filament. In all cases measured here, filamentary propagation is observed to cease shortly after the vacuum focus with only a small fraction of the total pulse energy absorbed. Our measurements suggest that the energy loss does not play a significant role in limiting filament length, because at filament termination, the pulses still contain energy well above the critical power for self-focusing, $P > P_{cr}$. Prior results [24] have shown that ~8 m propagation of a non-lens-assisted filament showed a loss of ~13% and that a lens placed in the beam path downstream of filament termination would initiate another filament. In our case, the dominant effect limiting the length of filaments appears to be divergence of the background reservoir, the region outside the filament core that exchanges energy with it [25,26]. Diffraction-limited focusing of an $f/600$ beam at $\lambda = 800$ nm would normally give a confocal parameter of $2z_0 \sim 60$ cm, which would roughly describe the axial extent of the high-intensity region of the filament reservoir. Nonlinear propagation of both the core and the reservoir extends this somewhat, as seen in the sonograms of Fig. 3, but the overall length scale of the filament conforms to the confocal parameter.

The depth of the gas density hole created by a single filament directly controls the index contrast between the core and cladding of the multi-filament-generated air waveguide [5], which in turn directly determines its numerical aperture. As seen from the results, increasing the pulse energy (intensity) in single filamentation increases the energy density absorbed by the propagation medium. Further increasing the energy, for example, in each lobe of a higher-order mode will eventually result in multi-filamentation, with the expectation that the energy absorption per filament will conform to our measurements. For example, in a scheme similar to [5,6], each filamenting lobe from a high-order Laguerre–Gaussian mode could be made energetic enough to induce multiple filamentation, raising the possibility of dramatically increasing the energy deposition, and thereby increasing the core–cladding index contrast in an air waveguide.

In conclusion, we have presented measurements of the energy deposited by a single filament for a range of laser energies and pulsewidths using two fully independent methods: measurements of absolute absorption, and inference of absorption using interferometric and sonographic measurements of the hydrodynamic response of air to the filament. Knowledge of the spatial distribution of energy deposition from filamentation will inform further study of filament-induced air waveguides, which show promise for long-range guiding of high-average-power lasers and remote collection of optical signals.

**Funding.** Air Force Office of Scientific Research (AFOSR) (FA95501310044); Army Research Office (ARO) (W911NF1410372); Defense Advanced Research Projects Agency (DARPA) (W911NF1410372).

**Acknowledgment.** The authors thank John Palastro (NRL) for useful discussions.

## REFERENCES

1. H. Pépin, D. Comtois, F. Vidal, C. Y. Chien, A. Desparois, T. W. Johnson, J. C. Kieffer, B. La Fontaine, F. Martin, F. A. M. Rizk, C. Potvin, P. Couture, H. P. Mercure, A. Bondiou-Clergerie, P. Lalande, and I. Gallimberti, Phys. Plasmas **8**, 2532 (2001).
2. P. B. Corkum, C. Rolland, and T. Srinivasan-Rao, Phys. Rev. Lett. **57**, 2268 (1986).
3. K. Stelmaszczyk, P. Rohwetter, G. Méjean, J. Yu, E. Salmon, J. Kasparian, R. Ackerman, J.-P. Wolf, and L. Wöste, Appl. Phys. Lett. **85**, 3977 (2004).
4. K. Y. Kim, J. H. Glownia, A. J. Taylor, and G. Rodriguez, Opt. Express **15**, 4577 (2007).
5. N. Jhajj, E. W. Rosenthal, R. Birnbaum, J. K. Wahlstrand, and H. M. Milchberg, Phys. Rev. X **4**, 011027 (2014).
6. E. W. Rosenthal, N. Jhajj, J. K. Wahlstrand, and H. M. Milchberg, Optica **1**, 5 (2014).
7. J. K. Wahlstrand, N. Jhajj, E. W. Rosenthal, S. Zahedpour, and H. M. Milchberg, Opt. Lett. **39**, 1290 (2014).
8. G. Point, C. Milian, A. Couairon, A. Mysyrowicz, and A. Houard, J. Phys. B **48**, 094009 (2015).
9. G. Point, E. Thouin, A. Mysyrowicz, and A. Houard, Opt. Express **24**, 6271 (2016).
10. A. A. Ilyin, S. S. Golik, and K. A. Shmirko, Spectrochim. Acta, Part B **112**, 16 (2015).
11. P. P. Kiran, S. Bagchi, C. L. Arnold, S. R. Krishnan, G. R. Kumar, and A. Couairon, Opt. Express **18**, 21504 (2010).
12. J. Kasparian, R. Sauerbrey, and S. L. Chin, Appl. Phys. B **71**, 877 (2000).
13. S. Zahedpour, J. K. Wahlstrand, and H. M. Milchberg, Phys. Rev. Lett. **112**, 143601 (2014).
14. N. H. Burnett and P. B. Corkum, J. Opt. Soc. Am. B **6**, 1195 (1989).
15. E. W. Rosenthal, J. P. Palastro, N. Jhajj, S. Zahedpour, J. K. Wahlstrand, and H. M. Milchberg, J. Phys. B **48**, 094011 (2015).
16. Y.-H. Cheng, J. K. Wahlstrand, N. Jhajj, and H. M. Milchberg, Opt. Express **21**, 4740 (2013).
17. S. Tzortzakis, B. Prade, M. Franco, and A. Mysyrowicz, Opt. Commun. **181**, 123 (2000).
18. Y.-H. Chen, S. Varma, A. York, and H. M. Milchberg, Opt. Express **15**, 11341 (2007).
19. D. V. Kartashov, A. V. Kirsanov, A. M. Kiselev, A. N. Stepanov, N. N. Bochkarev, Y. N. Ponomarev, and B. A. Tikhomirov, Opt. Express **14**, 7552 (2006).
20. J. Van Roey, J. van der Donk, and P. E. Lagasse, J. Opt. Soc. Am. B **71**, 803 (1981).
21. M. Takeda, H. Ina, and S. Kobayashi, J. Opt. Soc. Am. B **72**, 156 (1982).
22. P. E. Ciddor, Appl. Opt. **35**, 1566 (1996).
23. J. Yu, D. Mondelain, J. Kasparian, E. Salmon, S. Geffroy, C. Favre, V. Boutou, and J. P. Wolf, Appl. Opt. **42**, 7117 (2003).
24. W. Liu, Q. Luo, F. Théberge, H. L. Xu, S. A. Hosseini, S. M. Sarifi, and S. L. Chin, Appl. Phys. B **82**, 373 (2006).
25. A. Couairon and A. Mysyrowicz, Phys. Rep. **441**, 47 (2007).
26. M. Mlejnek, E. M. Wright, and J. V. Moloney, Opt. Lett. **23**, 382 (1998).